N95- 27632

SPACECRAFT MATERIALS STUDIES ON THE AEROSPACE CORPORATION TRAY ON EOIM-III

Wayne K. Stuckey, Carol S. Hemminger, Gary L. Steckel, Malina M. Hills, and Michael R. Hilton
Mechanics and Materials Technology Center
The Aerospace Corporation
2350 East El Segundo Blvd.
El Segundo, CA 90245
Phone: 310/336-7389, Fax: 310/336-5846

SUMMARY

A passive tray was flown on the Effects of Oxygen Interaction with Materials experiment on STS-46 (EOIM-III) with 82 samples from The Aerospace Corporation. A variety of advanced materials related to potential uses on future spacecraft were included for evaluation representing optical coatings, lubricants, polymers, composites, carbon-carbon composite protective coatings, graphite protective coatings, thermal-control materials, and some samples of current materials. An overview of the available results from the investigations of these materials is presented.

INTRODUCTION

The third experiment on the Effects of Oxygen Interaction with Materials (EOIM-III) was flown on STS-46. This mission was launched on July 31, 1992. On day 5, after deployment of Eureka and the tests of the Tethered Satellite System, the shuttle altitude was dropped to 124 nmi. The shuttle was oriented in a -Z orientation for 42 h, with the nose of the shuttle towards earth and the cargo bay into the velocity vector for the EOIM exposure to atomic oxygen. The fluence for the exposure was determined to be $2.3 \pm 0.1 \times 10^{20}$ oxygen atoms/cm^2 based on Kapton film erosion measurements, flux calculations using MSIS-86 with the as-flown orbit, and mass spectrometer measurements on EOIM-III.

The EOIM-III experiment submitted by The Aerospace Corporation consisted of one ambient-temperature tray with 82 samples (see Appendix I) and 19 samples placed on trays designed to have controlled temperature at 60°C, 120°C, and 200°C (see Appendix II). The actual temperatures from flight data showed that the ambient-temperature trays varied from 0°C to 43°C during the 42-h exposure, and the controlled-temperature trays were 58–80°C, 114–129°C, and 178–186°C.

The ambient-temperature tray was supplied by NASA-Johnson Space Center (ID No. 12). The samples were loaded into the tray at Aerospace and included a sample facing down in the tray as a flight control whenever possible. In addition, many samples had ground controls that were not flown. Many of the samples are vacuum-deposited coatings that did not initially experience additional vacuum conditioning upon receipt at Aerospace. The other samples had all experienced at least 24 h of 10^{-6} torr or less at room temperature. Many of the samples had also been in high-vacuum systems for pre-flight analyses by X-ray photoelectron spectroscopy (XPS) or scanning electron microscopy (SEM). Samples 22 and 23, with RTV 566 adhesive bonding silver interconnects, were held at 65°C for 24 h at pressures reaching into the 10^{-9} torr range. In response to a NASA request, the assembled tray with all samples except numbers 28, 29, 30 and 31 was placed in a vacuum chamber on a table maintained at 65–73°C for an additional 72 h. Pressures of $\sim 2.1 \times 10^{-6}$ torr were obtained initially and reached 5×10^{-8} at the conclusion of the bakeout. A residual gas analysis during the outgassing detected only water vapor. At room temperature, the final pressure was 5×10^{-9} torr. A Germanium ATR witness plate was placed in the chamber during the outgassing and showed

no detectable IR bands. Samples 28 and 29 were vacuum deposited and maintained at 65°C for 24 h with pressures of 2×10^{-8} to 5×10^{-9} torr. Samples 30 and 31 are typical optical components vacuum deposited by OCLI with preflight characterization that could not be repeated if included in the 65°C outgassing. All other samples, including all tray hardware, were included during the 65°C outgassing.

After the mission, the ambient tray was retrieved at NASA Kennedy Space Center and returned to Aerospace. Each sample was photographed immediately after removal from the tray. The controlled-temperature samples were removed from their fixture at NASA JSC and returned to Aerospace. The samples were then returned to the individual investigators for further study. Results on thermal-control materials are included elsewhere in these proceedings (ref. 1). Selected results will be presented here to give an overview of the results from the Aerospace tray.

RESULTS

Surface Contamination Analysis

Surface analysis by XPS of eight of the EOIM-III samples, which did not intrinsically contain silicon, listed in Table I, was used to evaluate surface contamination effects. Post-flight analysis of each sample was compared either to the pre-flight analysis results for the same sample, or to analysis of a ground-control sample made at the time of the post-flight analyses. A variety of surface changes was measured in the post-flight analyses, including contaminant deposition, surface oxidation, and surface stoichiometry changes. The major class of surface contaminant appears to have consisted of silicones. Surface silicon concentration increased from 4 to 11 atom % post-flight, with an average of 7 atom %. This implies the deposition of more than one monolayer of silicone on the flight-exposed samples.

The measured silicon concentrations were higher by a factor of 2 on the vanadium carbide samples located on the heated trays, compared to the silicon concentrations on the other samples in Table II located on the ambient-temperature tray. A quartz crystal microbalance experiment from NASA-Goddard located near the EOIM-III heated trays experienced significant weight gain on flight, which has not yet been

Table I. Silicon Concentration from XPS Analysis

Material	Atom %			
	Ground Control	Pre-flight Analysis	Post-flight Analysis	Increase in Si
SXA Mirror, E3-40	—	not detected	7.5	7.5
Cr on Graphite, E3-53	0.5	—	6.1	5.6
VC on Graphite, 60°C, E3-60-4	0.4	—	10	10
VC on Graphite, 120°C, E3-120-4	0.4	—	11	11
VC on Graphite, 200°C, E3-200-3	0.4	—	11	11
Anodized Al, E3-9†	—	5.7	11	5
ChemglazeA276, E3-25†	—	5.5	12	6
Z306, E3-10†	—	15	19	4

†Sample cut from exposed LDEF hardware, trailing edge.

completely explained. These data indicate the possibility for non-uniform contaminant deposition from localized sources on the EOIM-III experiment or from the Shuttle.

The contamination levels on the EOIM-III samples can be compared to those measured by XPS on a variety of LDEF samples (ref. 2). The average post-flight increase in silicon concentration for non-polymeric, leading-edge LDEF samples exposed for the duration of the mission was 17 atom %. By contrast, a nickel mirror sample exposed on-orbit only for 300 days had only a 2.5 atom % increase in Si surface concentration. This implies that both EOIM-III and LDEF samples may have received some silicone contamination from Shuttle sources.

Polymers

Polymers flown on the Aerospace EOIM-III experiment are shown in Table II. The atomic-oxygen erosion was determined by both weight loss measurements and profilometry. All of the samples were weighed pre-flight after conditioning to constant weight in a desiccator. Post-flight weights were measured in the same manner to determine the mass loss due to atomic-oxygen erosion of the polymer. In addition, an erosion step was formed by the beveled retainer ring on the front edge of the samples. This retainer created a protected and an exposed region that formed a circular crater on the sample. Surface profiles were determined with a Sloan Dektac 3030 at a minimum of three locations around the circumference of the crater to measure the step created from erosion of the polymer. There was good agreement between the two reactivity measurements. For reference, Kapton reactivity has been measured many times and is accepted to be 3.0×10^{-24} cm^3/O atom. The black Kapton included in this test was carbon-filled and consistently indicated a difference in reactivity between the old and new black Kapton obtained at different times. The measurements of the fluorinated polymers are slightly more variable.

Table II. Atomic Oxygen Erosion of Polymers

Material	Reactivity ($cm^3 \times 10^{-24}$/O Atom)	
	Profilometry	Weight
Black Kapton (Old)	2.1 ± 0.3	2.6
Black Kapton (New)	1.2 ± 0.1	1.0
6FDA + APB (spin)	2.6 ± 0.3	2.1
6FDA + APB (spray)	2.4 ± 0.6	1.6
6FDA + APB (both)	2.5 ± 0.5	1.85
6FDA + DDSO2	1.3 ± 0.3	0.3
BFDA + 4BDAF	2.3 ± 0.1	1.9
BTDA + 4,4ODA	3.4 ± 0.5	2.7

For the black Kapton samples, thermal property measurements were also performed (Table III). Some increase in solar absorptance was observed from erosion of the Kapton. The emissivity changes were slightly higher for the old black Kapton for the atomic-oxygen fluence experienced on EOIM-III, but no significant change was seen for the α/ε ratio.

Table III. Thermal Property Changes of Black Kapton on EOIM-III

Sample	Orientation in Tray	Solar Absorptance (α)	Emissivity (ε)	α/ε
"Old" Black Kapton	Up	0.988	0.928	1.06
"Old" Black Kapton	Down	0.930	0.887	1.05
"New" Black Kapton	Up	0.989	0.867	1.14
"New" Black Kapton	Down	0.929	0.871	1.07

Zinc Sulfide

Another EOIM-III experiment examined the oxidation of zinc-sulfide-coated lenses of an Earth-viewing sensor. Degradation of these lenses (loss of transmission at 14–16 μm) has been observed during solar maxima, when the density of atomic oxygen (AO) is highest. The degradation was, therefore, postulated to result from the interaction of AO with the lens material. In order to measure the kinetics of oxygen diffusion and reaction with the zinc sulfide coating, and thereby predict the extent of oxidation on the orbiting satellite, samples were flown on EOIM-III at three different temperatures:
ambient, 60°C, and 120°C.

The EOIM-III lens samples exhibited no change in their infrared optical properties. However, all lens samples exhibited extensive visible degradation in the area of AO exposure. X-ray photoelectron spectroscopic (XPS) measurements of the surfaces of the lens samples indicated that they were severely oxidized (see Table IV), and that the extent of oxidation increased with temperature. This temperature dependence suggests that the oxidation is diffusion-limited. Secondary Ion Mass Spectrometry (SIMS) of the lenses was also performed to measure the oxygen concentration profile as a function of depth. The SIMS data showed that the higher the temperature of the lens during the Shuttle exposure, the greater the depth of oxidation.

Table IV. Increase in oxygen content of zinc sulfide lens surfaces as determined by XPS.

Lens sample	Increase in Oxygen (atomic %)
Ambient #3	18
Ambient #4	16
60 °C	22
120 °C	31

Currently, the oxygen concentration data are being fit to a diffusion model. Preliminary modeling results suggest that the energy of diffusion is quite low ($E_{dif} < 10$ kcal/mole). The sensor lenses are exposed to a lower AO flux environment on the satellite than in the Shuttle bay, but are exposed to AO for a much longer period. The low energy of diffusion suggests that the extent of oxidation of the lenses on the satellite would be less than that observed on the EOIM-III samples. The lens degradation on the satellite would, therefore, have to be attributed to another degradation mechanism, such as contamination, or to synergistic effects such as simultaneous exposure to AO and UV light. (The lenses on the satellite were exposed to a higher intensity of UV light.) Completion of this modeling effort will clarify these results.

Optical Coatings

The optical coating configurations flown on the Aerospace tray are shown in Table V. Five of the samples were in virgin condition, and three received combined electron/proton/UV exposure in an experiment designed to ascertain the effect of on-orbit radiation on the optical and nuclear survivability of the coatings. These three samples were otherwise duplicates of three of the five virgin samples. The preconditioned samples received a dose of 2×10^{16} electrons/cm^2 at 40 keV, 3×10^{16} protons/cm^2 at 40 keV, and 1000 equivalent sun-hours UV exposure at a rate of 2 suns.

Companion samples to those flown on the Aerospace tray were tested at the atomic-oxygen exposure facility at Los Alamos National Laboratory. The fluence was 2×10^{20} atoms/cm^2 except for 240A-2, which received 1.8×10^{20} atoms/cm^2. The optical scatter from each sample was characterized before and after each atomic-oxygen exposure.

Comparison of the results of sample exposure on EOIM-III and at Los Alamos National Laboratory do not prove to be consistent. Two of the coating configurations show more scatter increase when fielded at

LANL, and four configurations showed greater increase on the EOIM-III experiment. However, many of these coatings also showed extensive deterioration of laboratory control samples (ref. 3).

Table V. Optical Coatings

Composition	EOIM-III Results	LANL Results
100 Å Al_2O_3 / 2400 Å BN // Fused Silica	Increase in scatter (129%) Blister diameter increase by 258% Slight erosion	Increase in scatter (111%) Blister diameter increase by 118% Slight erosion
100 Å Al_2O_3 / 2400 Å BN // FS (pre-exposed to e^-/UV/H^+)	Decrease in scatter (74%) Blister diameter increase by 223% Heavy erosion	No change in scatter (103%) No change in blister diameter Moderate erosion
2150 Å BN // Fused Silica	HUGE increase in scatter (261%) slight erosion	Increase in scatter (121%) Many small blisters
2150 Å BN // Fused Silica (pre-exposed to e^-/UV/H^+)	No change in scatter (103%) Moderate erosion	Increase in scatter (121%) Moderate erosion
1500 Å BN / 300Å Al // FS	Increase in scatter (141%) No erosion evident	No change in scatter (103%) Exposed area appears brighter No erosion evident
1500 Å BN / 300Å Al // FS (pre-exposed to e^-/UV/H^+)	Increase in scatter (116%) No erosion evident	Not tested
Magnesia-doped Al_2O_3 / SiO_2 Multilayer // FS	No change in scatter (99%) No other response	Not tested
200 Å SiO2 / 1000 Å TiN // FS	Increase in scatter (132%) No erosion evident	Increase in scatter (112%) No erosion evident

TiN and BN samples provided by Jaycor

Lubricants

Sputter-deposited MoS_2 lubricant films are used on a variety of spacecraft mechanisms, including release/deployment devices and some precision bearings. However, MoS_2 can oxidize into MoO_3, which is an inferior lubricant having low endurance and a relatively higher friction coefficient. Humid ground storage promotes oxidation (ref. 4). Atomic-oxygen exposure in ground tests has been found to cause surface oxidation to a depth of 9 nm (ref. 5). Most MoS_2 films have generally had as-deposited porous microstructures with (100) or (110) orientation. During sliding or rolling contact, lubricant particles would detach and reorient such that the (001) orientation (the active plane of slip) would become parallel to the surface. This burnished orientation is believed to have more oxidation stability. Films having dense, (001) oriented microstructures as-deposited have recently become available (ref. 6). These newer films were developed under BMDO auspices (PMA F1504 Materials and Structures Program) for precision gimbal bearings that would be used in sensor acquisition, tracking, and pointing mechanisms.

A series of MoS_2 films (deposited onto 440C steel) having different microstructures were flown on EOIM-III on several trays. The films were characterized structurally (SEM), chemically (AES/XPS), and tribologically (sliding friction coefficients in air and in UHV) by Sandia (PI: Michael T. Dugger) (ref. 7). Films having traditional (100)-oriented microstructures, prepared by Aerospace, were loaded onto a tray of the University of Alabama. Films with denser microstructures were flown on a JPL tray (Ovonics/OSMIC

0.7nm Ni/10nm multilayer MoS_2 film with 50 nm overlayer of pure MoS_2; Hohman cosputtered 20% SbO_x-MoS_2) or an Aerospace tray (Ovonics/OSMIC 0.9nm Au-20% Pd/10nm multilayer film with 50 nm overlayer of pure MoS_2; Naval Research Lab MoS_2 prepared using ion-beam-assisted deposition [IBAD]). All films were 1-μm thick. Duplicate samples were flown so that for each film type, one sample was exposed to AO, and one was shielded (flight control). Additional ground-control samples were prepared and characterized.

Post-flight analyses of these films are still in progress, though there is some preliminary data available (ref. 7). Of the newer films, microscopy has shown that the Ni-multilayer films exposed to flight AO have developed cracks and delaminated regions. The Au-multilayer (SbO_x-cosputtered) and the IBAD films did not have cracks or delaminated regions. Post-flight sliding tests in air have been conducted on these dense films. In the AO exposed regions, initial friction coefficients 3–4× above baseline were observed for the first 10 to 100 cycles before friction values dropped to baseline levels. The data suggests that a thin layer of MoO_3 had formed, which was quickly removed in sliding; this is consistent with the ground test AO experiments (ref. 5). From a design viewpoint, the preliminary data indicates that the Ni-multilayer films should be avoided for use as a lubricant on AO-exposed mechanisms because of coating fracture/delamination. The other dense lubricants may be more suitable for such mechanisms if the devices are not used continuously, although designers should anticipate higher initial friction coefficients after periods of inaction on exposed mechanisms if these lubricants are used. If the mechanisms are used continuously, these lubricants would appear to require shielding from AO to avoid continual oxide formation that would accelerate wear.

Composite Materials

Three composite samples were flown—two graphite-fiber-reinforced, polymer-matrix composites and one silicon-carbide, whisker-reinforced, metal-matrix composite. The metal-matrix composite was a flat mirror fabricated by Advanced Composite Materials Corporation (ACMC) and provided to NSWC. The mirror consisted of a low-density (0.42 g/cc) silicon carbide/aluminum (SiC/Al) foam core approximately 0.2-in. thick with SiC/Al surface foils. The 0.020-in. thick surface foils were applied with Sn96 Sn-Ag solder after an electroless nickel coating was applied to both bond surfaces. The planar mirror surface was then prepared by OCA Applied Optics. One of the SiC/Al face sheets was plated with an electroless nickel coating, which was polished to form the planar mirror finish. The final subsize mirror was 0.25-in. thick and 0.5-in. in diameter and had a density of approximately 2.0 g/cc.

The mirror surface was characterized preflight and postflight by total integrated scattering (TIS) to quantify its reflective properties and by XPS to determine the surface chemistry. The XPS data (see Table VI) provided evidence of several surface effects from the low earth orbit exposure, including contamination deposition, oxidation, and stoichiometry changes. Electroless nickel typically contains several percent phosphorous, which is in solution in the Ni or present as nickel phosphide, depending upon the concentration and heat treatment (ref. 8). The target phosphorous concentration for the mirror surface was relatively high (12 wt.%) so that a high fraction of Ni_3P would be expected. XPS indicated that the Ni:P atom ratio

Table VI. XPS Data for SXA Mirror, EOIM-III

	Surface Atom % (Normalized)									
	C	O	Si	Ni	P	N	S	Cl	Na	Ca
Pre-Flight	25	31	nd	29	13	nd	nd	nd	1.3	1.0
Post-Flight	16	53	7.5	21	0.5	nd	0.2	0.2	0.5	0.3

Note: nd = not detected and tr = trace.

on the surface changed from 2.2 preflight to 42 post-flight, while the phosphide-to-phosphate ratio changed from 2:1 to 1:1. These results indicate surface oxidation accompanied by a depletion of phosphorous from exposure to atomic oxygen. The extreme phosphorous depletion is assumed to result from the formation of volatile oxides and could lead to serious long-term surface degradation, such as pitting. SEM did not reveal any damage to the polished surface from the short-term EOIM-III exposure. However, atomic force microscopy performed by Advanced Materials Laboratory, Incorporated (ref. 9) gave indications of isolated pitting. Surface roughness measured over a 1-μm square was around 4 nm in the pitted areas versus less than 1 nm in typical areas. However, for most areas evaluated, the surface roughness was essentially the same in the exposed areas as in masked areas that were protected from atomic oxygen. The scattering measurements indicated that mirror performance was degraded. TIS increased by 100% from 0.0073 preflight to 0.0146 postflight, and the total hemispherical reflectance decreased by 7% from 0.537 to 0.498. Thus, some degradation of the mirror surface occurred and is probably related to the chemical changes. Similar results were reported (ref. 10) for polished electroless nickel surfaces flown on STS-5.

The polymer matrix composites included a P75S/934 graphite/epoxy composite with an eight-ply $(90/\pm30/90)_s$ lay-up and an AS4/PEEK graphite/thermoplastic composite with an eight-ply $(0/45/90/-45)_s$ lay-up. Mounted and polished cross sections were flown to obtain atomic-oxygen erosion surfaces in which the fibers and matrix were clearly distinguishable to serve as standards for the interpretation of LDEF erosion morphologies. Most polymer matrix composites flown on LDEF had either the coarse "Christmas tree" or cone-like structure exemplified by P75S/934 in Fig. 1a, or a fine, acicular structure as shown by Celion 6000/PMR-15 graphite/polyimide in Fig. 1b. The initial surfaces on LDEF samples were all as-fabricated surfaces so that it was not possible to distinguish between fiber and matrix areas on the eroded surfaces. Although it was not possible to identify parameters that controlled the erosion morphology, there did appear to be some correlation between the graphite-fiber type and the erosion features. Composites with higher-

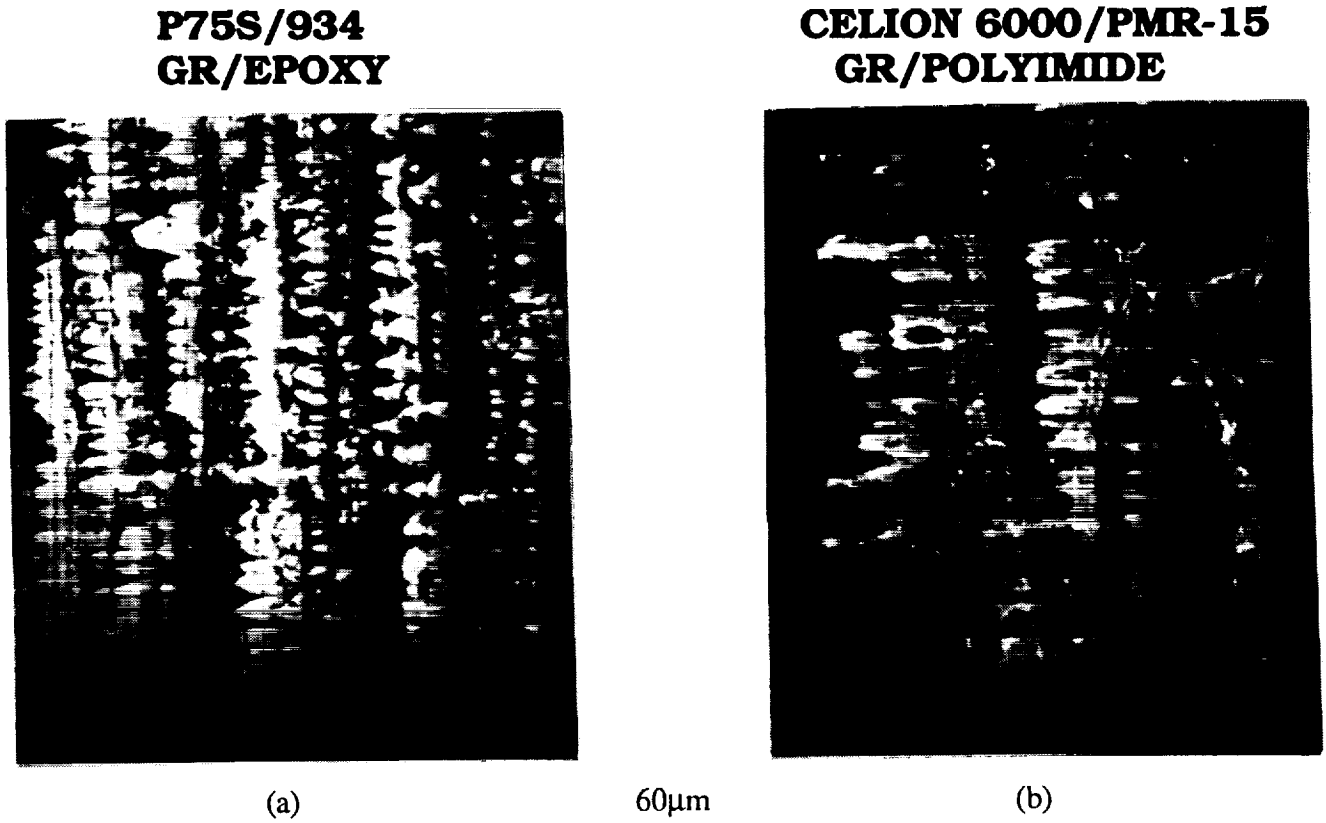

Figure 1. Scanning electron micrographs of atomic-oxygen erosion features of graphite-fiber-reinforced polymer matrix composites flown on LDEF.

modulus fibers (P75S and GY70) usually had the coarse Christmas tree features, while composites with lower-modulus fibers (Celion 6000 and T300) had the finer, acicular structure (ref. 11). Therefore, this experiment was performed to obtain controlled-erosion surfaces in which the fibers and matrix could be distinguished from each other. The composite systems were selected based on the differences between the relatively low modulus (34×10^6 psi), polyacrilonitrile-precursor AS4 fiber and the higher modulus (75×10^6 psi), mesophase pitch-precursor P75S fiber.

Several observations were made from SEMs of the erosion surfaces as shown in Fig. 2. The 934 epoxy and PEEK thermoplastic matrix erosion rates were significantly higher than those for the P75S and AS4 graphite fiber, respectively. The erosion morphologies were similar for the two polymer matrices. Similar erosion features were observed on the ends of the AS4 fibers, perpendicular to the fiber axis, and on the sides of the fibers, parallel to the fiber axis. Although not shown in Fig. 2, the P75S fiber also showed no orientation dependence for the erosion morphology. Finally, the P75S fiber eroded with a more uniform, finer structure than the AS4 fiber. This is contrary to the result anticipated from LDEF observations. Unfortunately, this experiment did not enable interpretation of LDEF atomic-oxygen erosion morphologies.

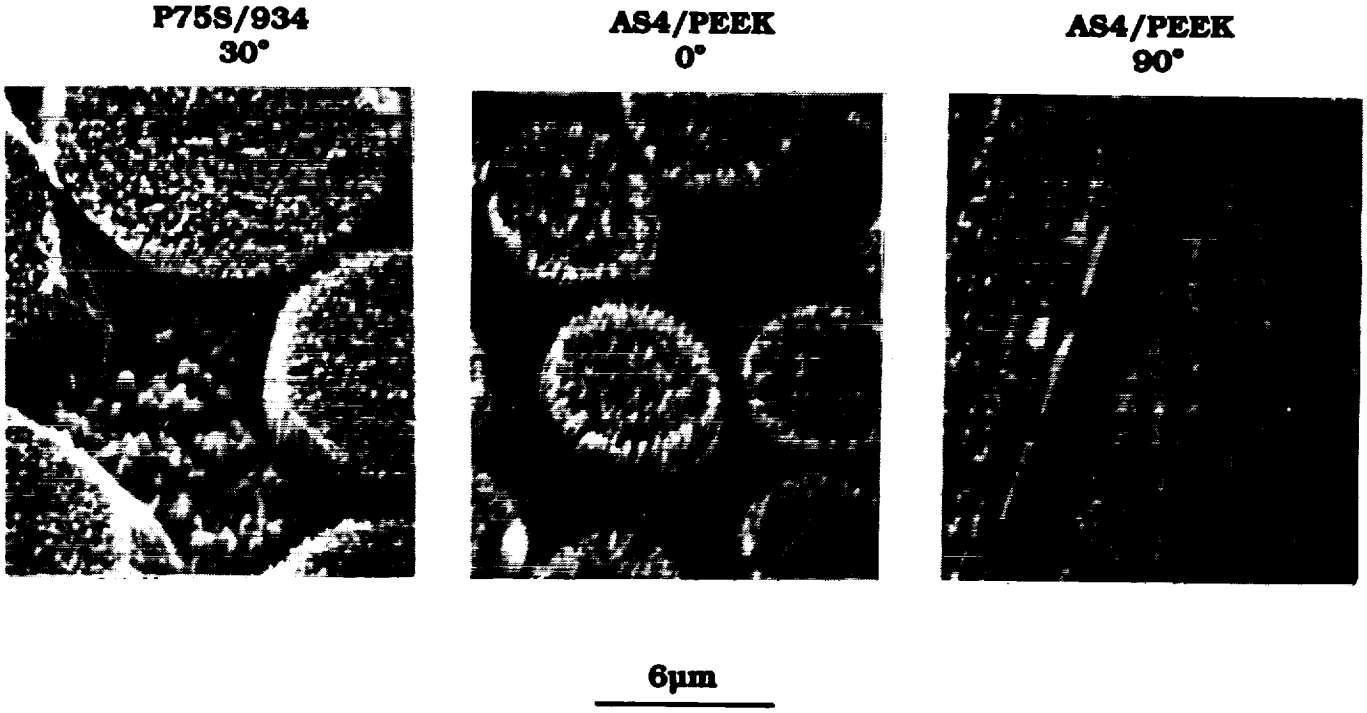

Figure 2. Scanning electron micrographs of atomic-oxygen erosion features for graphite-fiber-reinforced polymer matrix composites flown on EOIM-III. The fiber axis orientation relative to the atomic-oxygen velocity vector is shown for each micrograph.

Coated Graphite and Carbon-Carbon Samples

A variety of coatings over AXF-5Q polycrystalline graphite or carbon-carbon substrates was flown on the Aerospace ambient tray and the heated trays. The samples are described under sample numbers 45 through 64 in Appendix I for the ambient tray and the vanadium- and titanium-coated carbide samples on the heated tray summary in Appendix II. The carbide and boride coatings were deposited by CVD with ~100 μm thickness. Other coatings were either sputtered or deposited from a phosphoric-acid slurry. The reactivity of the uncoated carbon-carbon sample was indicated to be 1.4×10^{-24} cm^3/O Atom by weight-loss measurements. All of the coated specimens had reactivities at least a factor of 10 lower.

Three samples of ~1 μm chromium deposited on graphite were surface-analyzed by XPS: a ground control, a flight control (flown facing downward), and a flight exposed. The major surface changes observed were contaminant deposition and surface oxidation. The XPS composition data for the chromium-on-graphite samples is shown in Table VII. The major surface contaminants detected on the exposed sample were silicone and fluorocarbon residues. The silicon concentration was increased about 6 atom % relative to the ground and flight controls. The fluorine concentration was increased by a factor of 5 on both the flight control and flight exposed surfaces relative to the ground control. There was no evidence for fluorocarbon contamination greater than 1 atom % on the other EOIM-III flight samples analyzed by XPS in our laboratory. It is probable that the flight samples of chromium on graphite were contaminated pre-flight. The ground control had 4 atom % fluorine detected on its surface, indicating that variable levels of fluorocarbon contamination were deposited during fabrication or handling. A decrease in total surface carbon contamination was observed for the flight-exposed sample relative to the ground control, even with the deposition of silicone and fluorocarbon residues. This was typical of LDEF exposed surfaces as well (ref. 2) and is attributed primarily to volatilization of atomic oxygen reaction products such as CO and CO_2.

The increase in surface oxygen concentration by a factor of 2 on the flight sample relative to the ground control is due both to silicone contaminant residues and an increase in the surface oxidation of the chromium. XPS curve fit data for the $Cr2p_{3/2}$ peak of the three samples analyzed is shown in Table VIII. The flight-exposed surface has a significant decrease in the zerovalent chromium detected relative to the control surfaces. The peak attributed to CrO_2 and Cr_2O_3 increased on the exposed surface, and a new peak attributed to CrO_3 was also detected.

Table VII. XPS Composition Data for Chromium on Graphite Samples

Sample		Surface Atom %, Normalized								
		Cr	O	C	Si	F	N	Cl	Ca	Zn
	Ground Control	12	22	59	0.5	3.8	0.5	0.3	1.2	0.3
E3-53	Flown Down	10	27	35	0.6	25	0.6	0.7	0.8	0.2
E3-53	Exposed	6.7	41	26	6.1	19	1.0	0.2	0.6	0.2

Table VIII. $Cr2p_{3/2}$ Curve Fit Data for Chromium on Graphite EOIM-III Samples

Sample		$Cr2p_{3/2}$ Curve Fit Results, Normalized Percent		
		Zerovalent Cr	CrO_2, Cr_2O_3	CrO_3
	Ground Control	43	57	—
E3-53	Flown Down	36	64	—
E3-53	Exposed	9	70	21

Four samples of vanadium carbide on graphite were surface-analyzed by XPS: a ground control, and three flight-exposed samples from the 60°C, 120°C, and 200°C heated trays. The major surface changes observed were contaminant deposition and surface oxidation. The XPS composition data for the vanadium carbide on graphite samples is shown in Table IX. The major surface contaminants detected on the exposed sample were silicone residues. The silicon concentration was increased on the heated samples about 10 atom % relative to the ground control. This was a larger concentration increase than observed for flight-exposed samples of other material on the ambient-temperature tray of the experiment. The vanadium carbide films in this study were apparently not of high purity. Significant, but variable, concentrations of tantalum, tin, niobium, zirconium, and potassium were detected. It was not possible to deduce from the XPS data whether or not there were changes in the stoichiometry of the carbide film induced by the flight exposure since the extent of pre-flight composition variability was not known.

A decrease in total surface carbon concentration was observed for the flight-exposed samples relative to the ground control, even with the deposition of silicone residues. This indicates a loss of surface carbide and carbonaceous contamination by volatilization of atomic-oxygen reaction products such as CO and CO_2. The concentration of carbide carbon on the ground-control surface was about 6 atom % (determined by a curve fit of the C1s peak). Both vanadium and tantalum had surface carbide and oxide states present. The concentration of carbide carbon on the 60°C sample was about 0.5 atom %, and no carbide could be detected on the 120°C or 200°C sample surfaces. The metals were all detected predominantly as oxides on all three of the flight-exposed samples. The increase in surface oxygen concentration by a factor of 2 on the flight samples relative to the ground control is due both to silicone contaminant residues and an increase in the surface oxidation of the vanadium and other metals.

Table IX. XPS Composition Data for Vanadium Carbide on Graphite EOIM-III Samples

Sample		Surface Atom %, Normalized									
		V	C	O	Si	F	Ta	Sn	Nb	Zr	K
	Ground Control	8.3	61	25	0.4	0.4	4.4	0.4	0.8	0.1	nd
E3-60-4	Exposed, 60°C	10	13	65	10	0.3	0.4	0.1	0.1	0.3	0.2
E3-120-4	Exposed, 120°C	14	15	60	11	0.2	0.6	nd	tr	tr	0.1
E3-200-3	Exposed, 200°C	9.2	11	66	11	tr	2.2	0.1	0.4	tr	0.2

nd = not detected

tr = trace

Miscellaneous Samples

A variety of materials contributed by Hughes Space and Communications was flown on the Aerospace tray (ref. 12). Preliminary results are shown in Table X. Values shown for the solar absorptance and normal emittance are differences between the flight and control measurements. The value for the rhodium-plated molybdenum in the ambient tray was apparently the largest change, but an opposite trend was observed for the companion sample at 200°C. The erosion for the two polymeric resins was measured by microscopic examination.

Table X. Results on Hughes Space and Communications Samples

Sample Description	Sample Tray	Sample No.	Solar Absorptance Difference*	Normal Emittance Difference*	Measured Erosion (Microns)	Reaction Efficiency (cm^3/O Atom)
SPEREX Conductive Black Paint	Ambient	E3-75	-0.011	-0.039		
SPEREX Conductive Black Paint	200 °C	E3-200-5	-0.005	-0.053		
SPEREX White Paint, SP101	Ambient	E3-76	-0.009	-0.046		
SPEREX White Paint, SP101	200 °C	E3-200-6	0.021	-0.102		
Germanium/ Kapton	Ambient	E3-77	-0.005	-0.004		
Germanium/ Kapton	120 °C	E3-200-1	-0.003	-0.003		
Rhodium-Plated Molybdenum	Ambient	E3-77	0.090	0.002		
Rhodium-Plated Molybdenum	200 °C	E3-200-4	-0.064	-0.005		
954-3 Cyanate Ester Resin	Ambient	E3-78			6.0	2.6×10^{-24}
934 Epoxy Resin	Ambient	E3-79			6.5	2.8×10^{-24}

*Flown Value minus Control Value

SUMMARY

A variety of candidate spacecraft materials were flown on EOIM-III on the STS-46 shuttle mission. One full tray of 82 samples was flown at the ambient temperature during the mission, and samples were also on three trays held at fixed temperatures during the exposure. Results have been summarized on the observation of silicon contamination on the returned samples, the degradation of polymer samples, scatter properties of optical coatings, and the changes observed with zinc sulfide optical films, lubricants, composite materials, and coated carbonaceous materials.

Acknowledgments. The work on the silicon carbide/aluminum mirror and the coated graphite and carbon-carbon samples was supported by the Naval Surface Warfare Center. All other work reported was funded by the Air Force Materiel Command, Space and Missile Systems Center, under contract F04701-93-C-0094.

REFERENCES

1. M. J. Meshishnek and C. H. Jaggers, "Exposure of LDEF Materials to Atomic Oxygen: Results of EOIM-III," Third LDEF Post-Retrieval Symposium, November 8–12, 1993.

2. C. S. Hemminger, "Surface Contamination on LDEF Exposed Materials," LDEF Materials Workshop '91, NASA CP-3162, September, 1992, pp. 159–174.

3. M. L. Boeck and D. J. Speece, "Effect of Combined Electron/Proton/UV Exposure on Optical Coating Materials," TOR-93(3089)-2, The Aerospace Corporation, El Segundo, CA (15 May 1993).

4. P. D. Fleischauer, ASLE Trans, 27(1) (1983) 82.

5. J. R. Martin, J. B. Cross, and L. E. Pope, Mat. Res. Soc. Symp. Proc., 140 (1989) 271.

6. M. R. Hilton and P. D. Fleischauer, Surf. Coat. Technol., 54/55 (1992) 435.

7. Michael T. Dugger, Sandia National Laboratories, P. O. Box 5800, M/S 0340, Albuquerque, NM 87185-0340, Tel: 505-844-1091. Personal communication to M. R. Hilton, Aerospace Corp., 4/20/94.

8. The Engineering Properties of Electroless Nickel Deposits, International Nickel, The International Nickel Co., Inc., New York, NY, 1971.

9. T. L. Altshuler, "Atomic Force Microscopy of a Polished Nickel Plated Mirror EOIM3 E3-40 Exposed to Space on the August 1992 Shuttle Flight," Advanced Materials Laboratory, Inc. Report No. AML TR 93-13, May 6, 1993.

10. M. J. Meshishnek, W. K. Stuckey, G. S. Arnold, and D. R. Peplinski, "Effects on Advanced Materials: Results of the STS-8 EOIM Experiment," Atomic Oxygen Effects Measurements for Shuttle Missions STS-8 and 41-G, NASA Technical Memorandum 100459, Vol. II, pp. 5–6, Sept. 1988.

11. G. L. Steckel, T. Cookson, and C. Blair, "Polymer Matrix Composites on LDEF Experiments M0003-9 & 10," LDEF Materials Workshop '91, NASA CP-3162, pp. 515–542, 1992.

12. Bruce Drolin, private communication, Hughes Space and Communications, El Segundo, CA.

APPENDIX I. AMBIENT EOIM-III TRAY - THE AEROSPACE CORPORATION

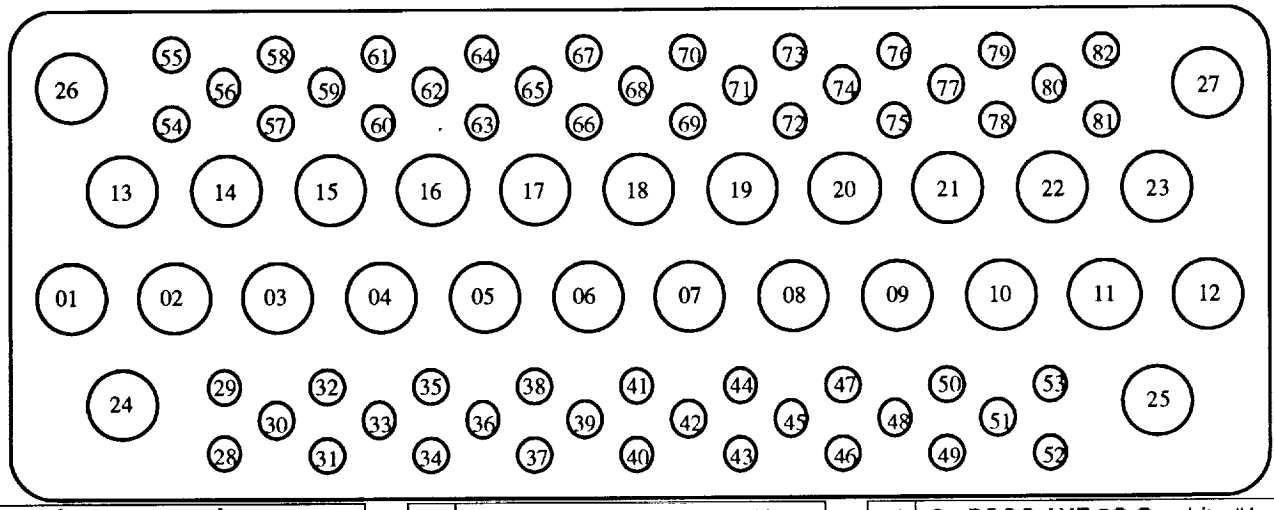

1	100 Å Al_2O_3 / 2400 Å BN // Fused Silica (exposed to e^- /UV/H^+) #SE1-01
2	100 Å Al_2O_3 / 2400 Å BN // Fused Silica #SE1-05
3	2150 Å BN // Fused Silica (exposed to e^-/UV/H^+) #SE2-01
4	2150 Å BN // Fused Silica #SE2-05
5	1500 Å BN / 300Å Al // Fused Silica (exposed to e^-/UV/H^+) #6A7-5
6	1500 Å BN / 300Å Al // Fused Silica #6A7-3
7	Magnesia-doped Al_2O_3 / SiO_2 Multilayer // Fused Silica #B-1
8	200 Å SiO_2 / 1000 Å TiN // Fused Silica #SE5-02
9	LDEF Anodized Aluminum # 1-1
10	LDEF Z306 #4-1
11	LDEF S13GLO Leading Edge #3-1
12	LDEF S13GLO Trailing Edge #2-1
13	Ovonics Au-MoS_2 multilayer film on 440C steel #071091-013
14	Ovonics Au-MoS_2 multilayer film on 440C steel #071091-015
15	NRL MoS_2 films #102591-002
16	NRL MoS_2 films #102591-004
17	Diamond-like Film (C) #071091-003/Ag Mask
18	Diamond-like Film (C) #071091-009/Ag Mask
19	Black Kapton- Old #1
20	Black Kapton-New #1
21	Germanium/Kapton
22	Silver Interconnect
23	Silver Interconnect

24	Anodized&Nickel Plated/ SiC-Aluminum
25	LDEF A276 Trailing Edge #1-1
26	6FDA + APB Spin Coated #1
27	6FDA + APB Spray Coated #1
28	Fluorinated Corning 7940
29	Fluorinated Corning 7940
30	Ambient Lens 3
31	Ambient Lens 4
32	ZnS/Silicon #ZnS-5
33	ZnS/Silicon #ZnS-7
34	TiO_2/Silicon #MOCVD 92-111
35	TiO_2/Fused Silica #MOCVD 92-112
36	TiO_2/Involute Carbon-Carbon #MOCVD 92-114
37	TiO_2/Braided Carbon-Carbon #MOCVD 92-115
38	TiO_2/POCO Graphite #MOCVD 92-116
39	TiO_2-SiO_2/Silicon #MOCVD 92-117
40	Nickel Plated/ SiC-Aluminum Mirror
41	Silicon Carbide Mirror
42	P75/934 Graphite Epoxy
43	AS4/PEEK
44	6FDA + $DDSO_2$ #1
45	TiC / POCO AXF-5Q Graphite #1
46	VC / POCO AXF-5Q Graphite #1
47	TiB_2 /POCO AXF-5Q Graphite #1
48	TiC / POCO AXF-5Q Graphite #1
49	NiAl #1
50	NiBe/POCO AXF-5Q Graphite #1
51	Ti_2Be_{17} / POCO AXF-5Q Graphite #1
52	V / POCO AXF-5Q Graphite #1

53	Cr/ POCO AXF-5Q Graphite #1
54	Si&SiC / Carbon-Carbon #1
55	SiO_2 /Si&SiC/Carbon-Carbon #1
56	Al_2O_3/Si&SiC/Carbon-Carbon #1
57	Rh/Si&SiC/Carbon-Carbon #1
58	ZrP_2O_7 / Carbon-Carbon #1
59	SiO_2/ZrP_2O_7/Carbon-Carbon #1
60	SiP_2O_7/Carbon-Carbon #1
61	SiO_2/SiP_2O_7/Carbon-Carbon #1
62	Carbon-Carbon Composite #1
63	$AlPO_4$ / Carbon-Carbon #1
64	SiO_2/$AlPO_4$ / Carbon-Carbon #1
65	NRL Diamond-like Film (Si) #"D"
66	NRL Diamond-like Film (Si) #1
67	BFDA + 4BDAF #1
68	6FDA + APB Spin Coated #1
69	6FDA + APB Spray Coated #1
70	BTDA + 4,4ODA #1
71	Liquid Crystalline Epoxy/PDA
72	EPON 825/PDA
73	Vectra 4950 Liquid Crystalline Polymer
74	XYDAR SRT 300 Liquid Crystalline Polymer
75	Sperex Conductive Black Paint
76	Sperex White Paint SP101
77	Rhodium-plated Molybdenum
78	954-3 Cyanate Ester
79	934 Epoxy
80	High Temperature Adhesive
81	CV1144 Protective Silicone on Gr/Ep
82	AO Resistant Polyimide

APPENDIX II. HEATED SAMPLE CARRIER SUMMARY - THE AEROSPACE CORPORATION

Number	Size	Material	Investigator
		60 °C Tray	
E3-60-1	1"	Germanium/ Kapton	Drolin
E3-60-2	1"	Solar Cell Interconnect Silver #11	Drolin
E3-60-3	0.5"	Lens 1	Hills
E3-60-4	0.5"	VC/Graphite	Foltz/Opeka
E3-60-5	0.5"	TiC/Graphite	Foltz/Opeka
E3-60-6	0.5"	CV1144 Silicone on Gr/Ep	Drolin
E3-60-7	0.5"	Silicone/Polyimide (Unannealed)	Gilman
E3-60-8	0.5"	Silicone/Polyimide (Annealed)	Gilman
		120 °C Tray	
E3-120-1	1"	Germanium/ Kapton	Drolin
E3-120-2	1"	Solar Cell Interconnect Silver #6	Drolin
Lens 1	0.5"	Lens 2	Hills
E3-120-4	0.5"	VC/Graphite	Foltz/Opeka
E3-120-5	0.5"	Silicone/Polyimide (Unannealed)	Gilman
E3-120-6	0.5"	Silicone/Polyimide (Annealed)	Gilman
		200 °C Tray	
E3-200-1	1"	-	-
E3-200-2	1"	Solar Cell Interconnect Silver #8	Drolin
E3-200-3	0.5"	VC/Graphite	Foltz/Opeka
E3-200-4	0.5"	Rhodium-plated Molybdenum	Drolin
E3-200-5	0.5"	SPEREX Black	Drolin
E3-200-6	0.5"	SPEREX White	Drolin